Electronic Supplementary Material (ESI) for ChemComm.
This journal is © The Royal Society of Chemistry 2016

Electronic Supplementary Information (ESI†)

Controlled Synthesis and Comparison of $NiCo_2S_4$/graphene/2D TMDs Ternary Nanocomposites for High-performance Supercapacitors

Jianfeng Shen[1], Pei Dong[2], Robert Baines[2], Xiaowei Xu[1], ZhuQing Zhang[1], Pulickel M. Ajayan[2], Mingxin Ye[1]*

[1] Institute of special materials and technology, Fudan University, 200433, Shanghai, China

[2] Department of Materials Science and NanoEngineering, Rice University, 6100 Main Street, Houston, TX 77005, USA

Materials

MoS_2 (99%) and $MoSe_2$ (99.9%) were supplied by Sigma-Aldrich. All the other chemicals were of analytical level and used as received. All aqueous solutions were prepared with ultrapure water from a Milli-Q Plus system.

Preparation of $NiCo_2S_4$-g-TMDs

In a typical synthesis of $NiCo_2S_4$-g-TMDs nanocomposite (take $NiCo_2S_4$-g-$MoSe_2$ as the example), firstly, 90 milligrams of graphite and $MoSe_2$ were added to a 50 mL glass vial [1, 2]. After that, 30 mL of 1:1 isopropanol (IPA)/water was added. The mixture was then sonicated with a frequency of 40 kHz for 4 h. Subsequently, the mixture was centrifuged at 1000 r.p.m. for 10 min. The supernatants were collected and centrifuged at 4000 r.p.m. for another 10 min to remove non-exfoliated materials. Second, 2 mmol $Co(NO_3)_2 \cdot 6H_2O$, 1 mmol $NiCl_2 \cdot 6H_2O$, and 9 mmol thiourea were dissolved in a 25 mL exfoliated $MoSe_2$ solution (IPA/water 1:1) and 25 mL of graphene solution (IPA/water 1:1). 1 mL of ammonia was added dropwise to the

solution. The mixture was magnetically stirred for 1 h and then sonicated for 1h. Next, the mixture was transferred into a Teflon-lined autoclave, sealed, and heated at 200 °C in an oven for 24 h. The product was filtered, washed with water and ethanol for three times each, and dried in vacuum at 60 °C for 12 h. As for $NiCo_2S_4$-g: no $MoSe_2$ was added. For the preparation of $NiCo_2S_4$-g-MoS_2, $MoSe_2$ was replaced with MoS_2 (exfoliated in 7:3 IPA/water). The whole process is illustrated in Figure 1.

Materials characterization

The surface morphologies of the fabricated nanocomposites were examined with a field-emission scanning electron microscope (FEI Quanta 400 ESEM FEG), including element mapping. As well, transmission electron microscope (TEM) and high-resolution TEM (HRTEM) images were obtained using a JEOL 2010, with an acceleration voltage of 200 kV. AFM images were acquired with the equipment of Bruker Multimode 8. X-ray photoelectron spectra (XPS) were observed on a PHI Quantera X-ray photoelectron spectrometer. Powder X-ray diffraction (XRD) analyses were performed on a Bruker D8 Advance diffractometer with Cu and Ka radiation. Raman spectra were recorded from 100 to 4000 cm^{-1} on a Renishaw Invia Raman Microprobe, using a 514.5 nm argon ion laser. TGA was carried out with TA Q-600, from ambient temperature to 600 ºC, at 10 ºC/min heating rate, under argon atomosphere. UV-Vis diffusive reflection spectra were carried out on a Shimadzu UV-3600 spectrophotometer.

Working electrodes fabrication and electrochemical measurements

Autolab 302 electrochemical workstation was used to characterize the electrochemical behaviors. In half-cell test, three-electrode glass cell with 6 M KOH as the aqueous electrolyte was conducted. 80 wt% active materials, 10 wt% carbon black and 10 wt% polyvinylidene fluoride were mixed together. Then the mixture was

further dispersed in N-methyl-2-pyrrolidone to form the homogeneous slurry which was pasted on nickel foams. After that, the foams dried at 120 ºC for 12 h in a vacuum oven and the dried nickel foams were pressed to be a thin foil at a pressure of 10 MPa for 1 min. Cyclic voltammograms (CVs) and Galvanostatic charge-discharge (GCD) curves were measured with an electrochemical analyzer (Autolab 302) in 6 M KOH. The reference and counter electrodes were Ag/AgCl and platinum plate, respectively. CV curves were obtained at various scan rates (5, 10, 20, 50 and 100 mV s^{-1}) in a potential window of 0-0.6 V. GCD curves were recorded at various current densities (1, 2, 5, 10 and 20 A g^{-1}) in a potential window of 0-0.4 V. While in full cell test, the symmetric supercapacitor cell using filter paper as the separator was assembled to measure the device performances. The loading mass of the active materials was controlled to be about 5 mg, with the surface area of 1 cm^2 for each working electrode.

Calculation of capacitance

Observing CV measurements, the capacitance (Cm, F g^{-1}) of the measured materials was calculated according the following equation:

$$C_m = \frac{\int I(V)dv}{vm\Delta V} (F\,g^{-1})$$

where m is the total mass of the electroactive material (g), v is the scan rate (V s^{-1}), and ΔV is the potential window (V).

For the specific capacitance calculation we used the GCD curves. The measured capacitance (Cm) can be calculated as:

$$C_m = \frac{I\Delta t}{m\Delta V} (Fg^{-1})$$

where I is the discharge current (A), and Δt is the discharge time (s).

As for the prepared symmetric supercapacitor,

$$E = \frac{1}{2}(\frac{1000}{3600})CV^2$$

$$P = \frac{E}{t_d}$$

Supplementary figures and discussion

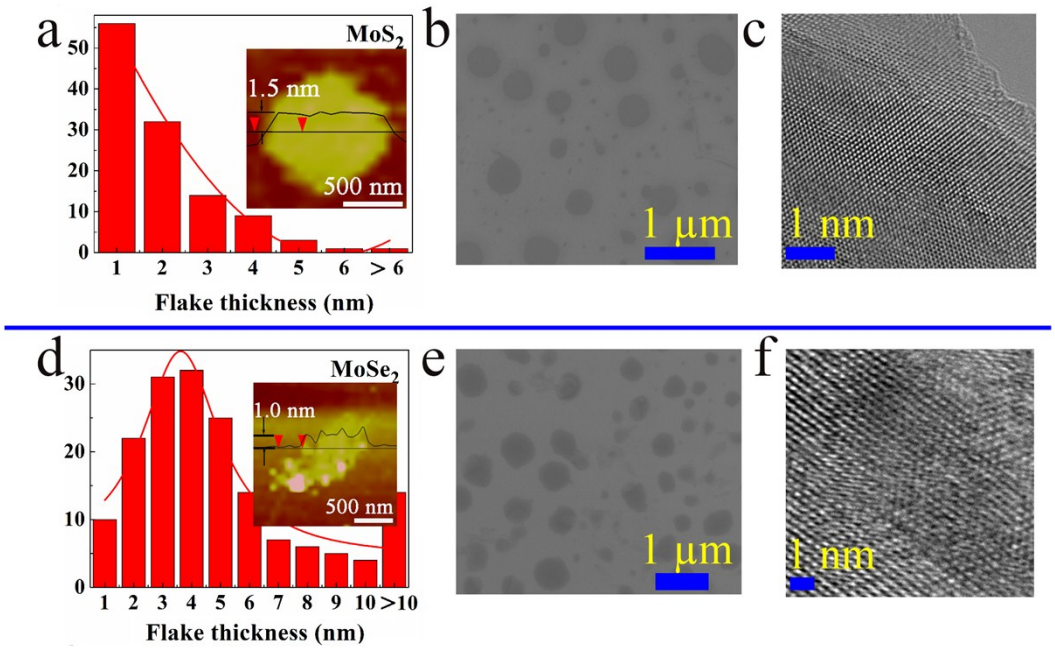

Figure S1 AFM, SEM and High resolution TEM images of MoS_2 (a, b, c), and $MoSe_2$ (d, e, f) nanosheets.

More than 100 MoS_2 and $MoSe_2$ nanosheets were randomly selected and analyzed with AFM to obtain the distribution of their thickness. It can be found that most of the MoS_2 and $MoSe_2$ nanosheets have few layers. Moreover, SEM and TEM images demonstrated that these MoS_2 and $MoSe_2$ nanosheets were with reduced lateral sizes, but still remain good crystal structure, which is also consistent with XRD results.

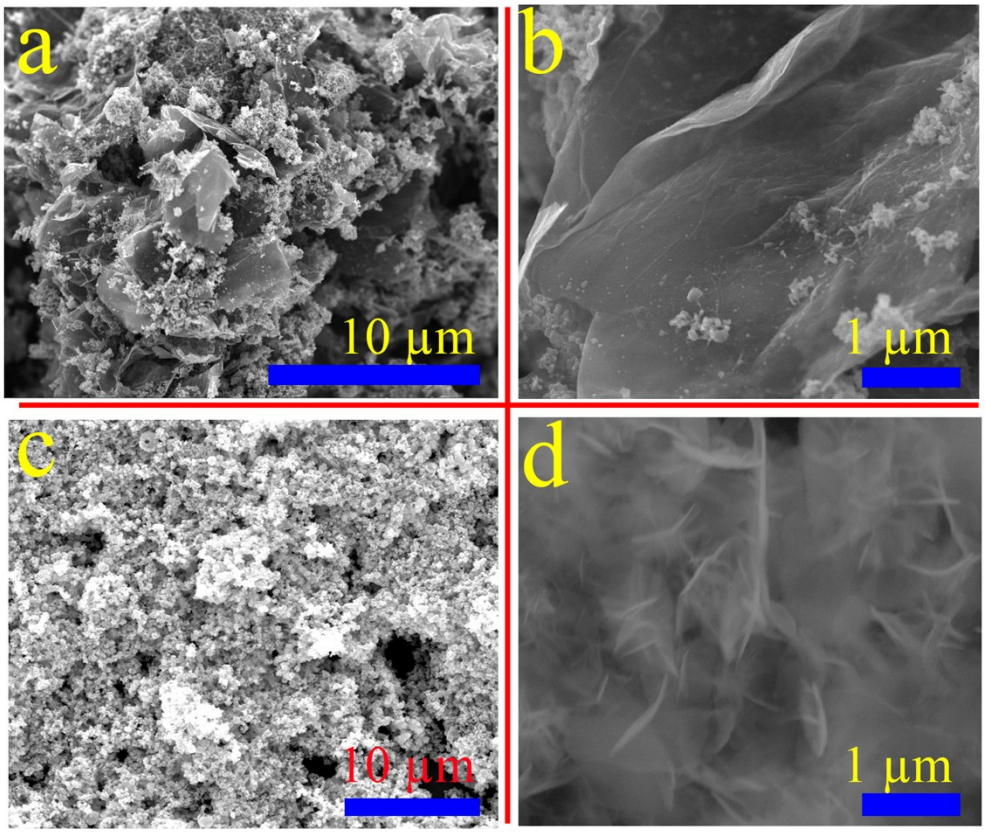

Figure S2. Low and high resolution SEM images of $NiCo_2S_4$-g (a, b) and $NiCo_2S_4$-g-$MoSe_2$ (c and d)

On one hand, it is found that $NiCo_2S_4$-g-$MoSe_2$ and $NiCo_2S_4$-g-MoS_2 have similar morphological structures, thus the difference of electrochemical properties of these $NiCo_2S_4$-g-TMDs mainly originates from the basic properties of the TMDs. On the other hand, it can be found that the addition of MoS_2 or $MoSe_2$ nanosheets will have great effect on the morphology of the nanocomposites. This phenomenon is interesting and it is consistent with the electrochemical properties that the $NiCo_2S_4$-g-TMDs have much higher capacitances than that of $NiCo_2S_4$-g.

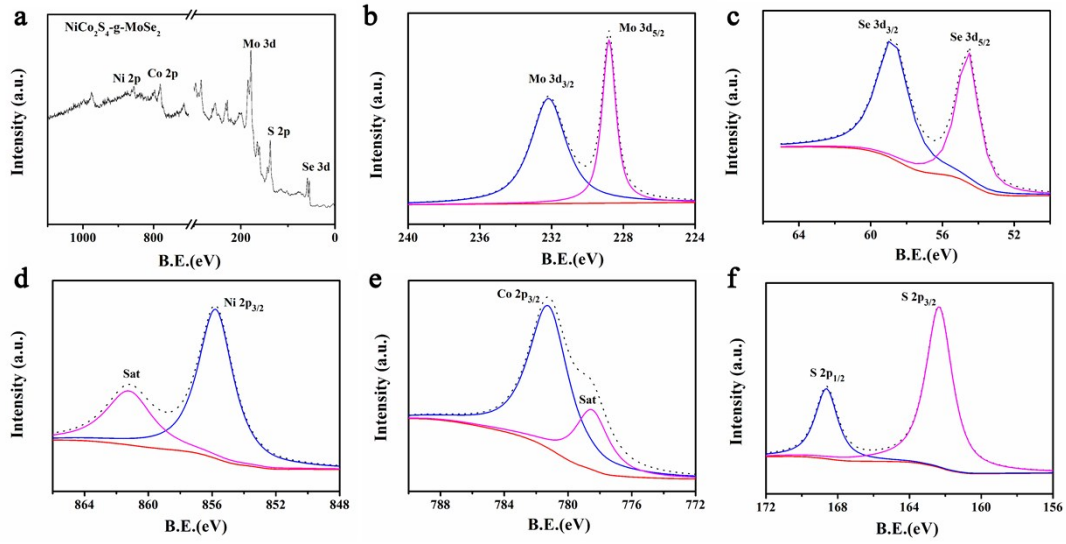

Figure S3. XPS survey spectrum of $NiCo_2S_4$-g-$MoSe_2$ (a). High-resolution XPS spectra of Mo 3d (b), Se 3d (c), Ni 2p (d), Co 2p (e), and S 2p (f) of $NiCo_2S_4$-g-$MoSe_2$.

The XPS survey spectrum of $NiCo_2S_4$-g-$MoSe_2$ (Figure S3a) indicates that C, Ni, S, Mo, and Se elements exist in the sample. From the integration of the elements peaks, the atomic ratios of Ni: Co: S: Mo: Se: C were around 1: 1.90: 3.75: 0.92: 1.81: 6.04. Figure S3b demonstrates the two peaks at 229.0 and 232.1 eV attributed to the doublets $Mo3d_{5/2}$ and Mo $3d_{3/2}$[3]. Se $3d_{5/2}$ and Se $3d_{5/2}$ can be clearly found at 54.2 and 58.4 eV (Figure S3c)[4]. The Ni 2p spectrum (Figure S1d) can be best fitted by Ni $2p_{3/2}$and its shake-up satellite[5]. Similarly, Figure S3e indicates the energy band (Co $2p_{3/2}$) and its satellite peak[6]. S 2p spectrum (Figure S1f) is divided into two main peaks (S $2p_{1/2}$ and S $2p_{3/2}$ at 162.1 and 168.5 eV). These peaks can be attributed to the metal-sulfur bonds in low coordination at the surface[7].

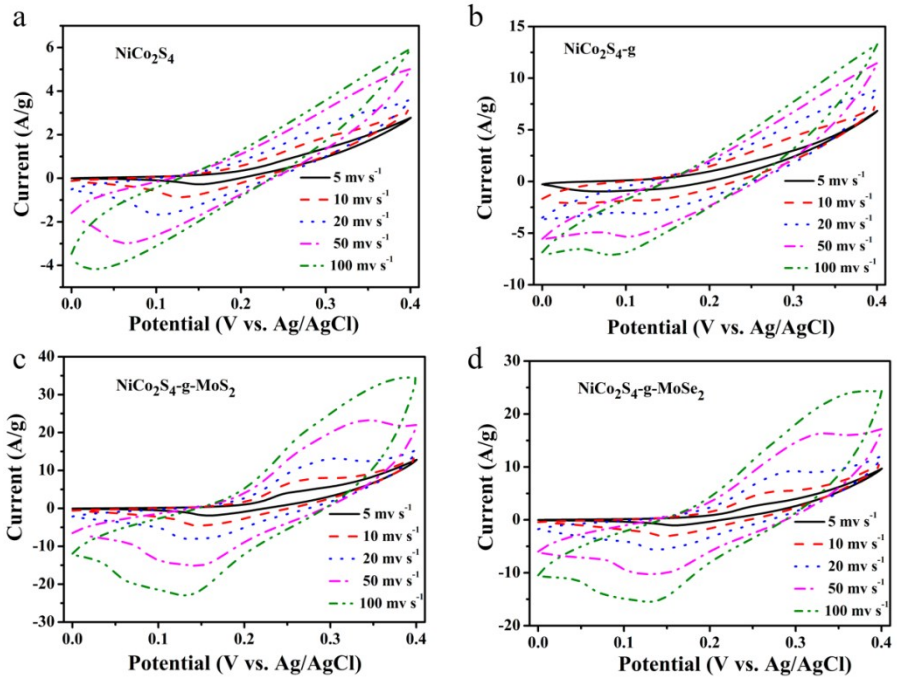

Figure S4. CV curves of $NiCo_2S_4$, $NiCo_2S_4$-g, $NiCo_2S_4$-g-MoS_2, and $NiCo_2S_4$-g-$MoSe_2$ at different scanning rates.

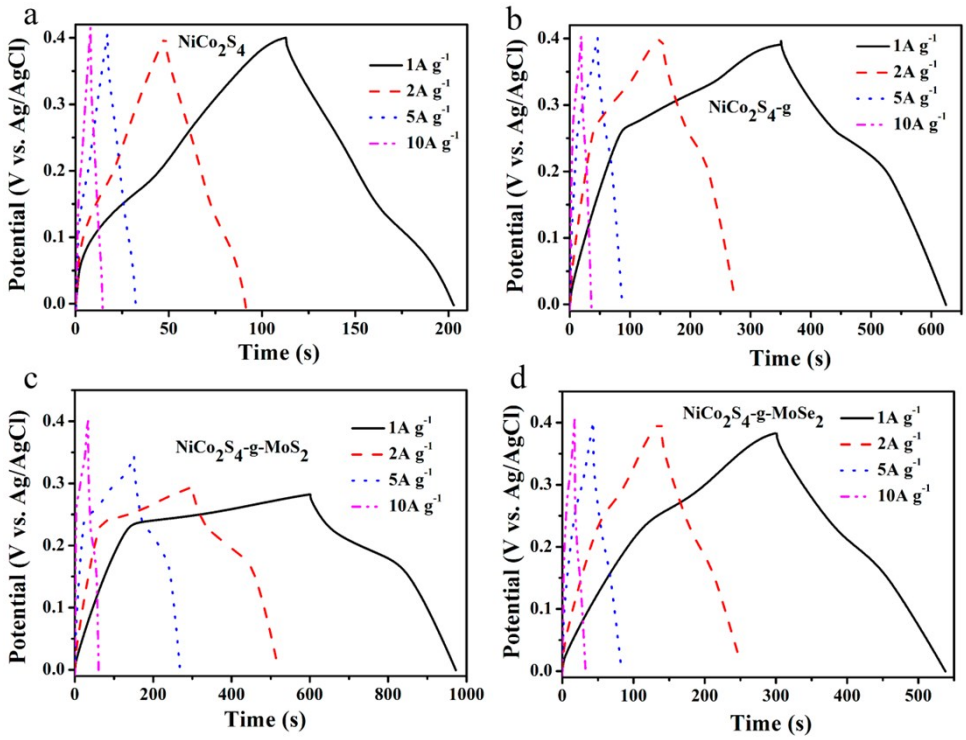

Figure S5. GCD curves of $NiCo_2S_4$, $NiCo_2S_4$-g, $NiCo_2S_4$-g-MoS_2, and $NiCo_2S_4$-g-$MoSe_2$ at different current densities.

References:

1. J. Shen, Y. He, J. Wu, C. Gao, K. Keyshar, X. Zhang, Y. Yang, M. Ye, R. Vajtai, J. Lou and P. M. Ajayan, *Nano Letters*, 2015, **15**, 5449-5454.

2. J. N. Coleman, M. Lotya, A. O'Neill, S. D. Bergin, P. J. King, U. Khan, K. Young, A. Gaucher, S. De, R. J. Smith, I. V. Shvets, S. K. Arora, G. Stanton, H.-Y. Kim, K. Lee, G. T. Kim, G. S. Duesberg, T. Hallam, J. J. Boland, J. J. Wang, J. F. Donegan, J. C. Grunlan, G. Moriarty, A. Shmeliov, R. J. Nicholls, J. M. Perkins, E. M. Grieveson, K. Theuwissen, D. W. McComb, P. D. Nellist and V. Nicolosi, *Science*, 2011, **331**, 568-571.

3. S. Patil, A. Harle, S. Sathaye and K. Patil, *CrystEngComm*, 2014, **16**, 10845-10855.

4. H. Zhang, B. Yang, X. Wu, Z. Li, L. Lei and X. Zhang, *ACS Applied Materials & Interfaces*, 2015, **7**, 1772-1779.

5. V. H. Nguyen and J.-J. Shim, *Journal of Power Sources*, 2015, **273**, 110-117.

6. W. Hu, R. Chen, W. Xie, L. Zou, N. Qin and D. Bao, *ACS Applied Materials & Interfaces*, 2014, **6**, 19318-19326.

7. Y. Zhang, W. Sun, X. Rui, B. Li, H. T. Tan, G. Guo, S. Madhavi, Y. Zong and Q. Yan, *Small*, 2015, **11**,3694-3702.